



DEGREE PROJECT IN MEDICAL ENGINEERING,  
SECOND CYCLE, 30 CREDITS  
*STOCKHOLM, SWEDEN 2020*

# **Designing a fast and robust device for measuring and providing graphical visualization of the number of $^{60}\text{Co}$ sources in a Leksell Gamma Knife<sup>®</sup>**

Designa en snabb och robust anordning för att  
mäta och tillhandahålla grafisk visualisering av  
antalet  $^{60}\text{Co}$  källor i en Leksell Gamma Knife<sup>®</sup>

**SIMON ANDERSSON**



# **Designing a fast and robust device for measuring and providing graphical visualization of the number of $^{60}\text{Co}$ sources in a Leksell Gamma Knife<sup>®</sup>**

SIMON ANDERSSON

Master in Medical Engineering

Date: August 13, 2020

Supervisor: Per Kjäll

Reviewer: Massimiliano Colarieti Tosti

Examiner: Matilda Larsson

School of Engineering Sciences in Chemistry, Biotechnology and Health

Host company: Elekta Instrument AB

Swedish title: Designa en snabb och robust anordning för att mäta och tillhandahålla grafisk visualisering av antalet  $^{60}\text{Co}$  källor i en Leksell Gamma Knife<sup>®</sup>



## **Abstract**

The Leksell Gamma Knife<sup>®</sup> (LGK) is a device for performing radiosurgery. The LGK contains approximately 200 radioactive sources whose beams intersect in a focal point in order to treat brain tumours. Quality assurance tools are used at Elekta to indirectly assess the number of sources in an LGK from the total amount of radiation. In order to increase patient safety, regulatory agencies have been asking for evidential proof of the number of sources in the LGK. This thesis' goal is to directly measure each source in the LGK and optimize the total detection time. To do this, a source detection system was developed with two parts, a radiation detection system and a moving gantry. Initial tests of the design were performed at Elekta and a final test was performed on an LGK at Karolinska Universitetssjukhuset. The results show that the proposed design has the possibility of detecting all sources in an LGK.

## Sammanfattning

Leksell Gamma Knife® (LGK) är en apparat för att utföra strålkirurgi. LGK innehåller cirka 200 radioaktiva källor vars strålar korsar varandra i en fokuspunkt för att behandla hjärntumörer. Kvalitetssäkringsverktyg används av Elekta som indirekt kan bedöma antalet källor i en LGK utifrån den totala strålmängden. För att öka patientsäkerheten har tillsynsmyndigheter begärt bevis för antalet källor i LGK. Målet för denna avhandling är att direkt mäta varje källa i LGK och optimera den totala detekteringstiden. För att göra detta utvecklades ett källdetekteringssystem med två delar, ett för strålningsdetektering och ett för motorstyrning. Inledande tester av designen utfördes på Elekta och ett slutligt test utfördes på en LGK på Karolinska Universitetssjukhuset. Resultaten visar att den föreslagna designen har möjlighet att detektera alla källor i en LGK.

## Acknowledgements

I would first like to thank Elekta Instrument AB for the opportunity of doing my thesis at the company. Apart from this I would like to give a huge thank you to Per Kjäll for presenting the topic to me as well as guiding me throughout the process of this thesis. I would also like to thank Anton Karlberg for assisting me for these months. Lastly, I want to thank Massimiliano Colarieti Tosti for being my reviewer and for his constructive criticism throughout this process. Lastly, an enormous thank you to my family and friends, without you I would not have come this far.

## Abbreviations

$^{60}\text{Co}$	Cobalt-60
Elekta	Elekta Instrument AB
EtherCAT	Ethernet for Control Automation Technology
LGK	Leksell Gamma Knife <sup>®</sup>
PLC	Programmable Logic Controller
PPS	Patient Positioning System
TwinCAT	The Windows Control and Automation Technology

# Contents

<b>1</b>	<b>Introduction</b>	<b>1</b>
1.1	Goal of thesis . . . . .	2
<b>2</b>	<b>Methods and materials</b>	<b>3</b>
2.1	Source detection system . . . . .	3
2.1.1	Radiation detection . . . . .	4
2.1.2	Moving gantry . . . . .	6
2.2	Testing at Elekta Instrument AB . . . . .	6
2.2.1	Collimator testing . . . . .	7
2.2.2	Velocity testing . . . . .	8
2.2.3	Acquisition time testing . . . . .	8
2.2.4	Precision testing . . . . .	8
2.3	Parameter selection . . . . .	8
2.4	Testing at Karolinska Universitetssjukhuset, Solna . . . . .	10
2.4.1	Calculating coordinates for calibration . . . . .	10
<b>3</b>	<b>Results</b>	<b>13</b>
3.1	Collimator testing . . . . .	13
3.2	Velocity testing . . . . .	14
3.3	Acquisition time testing . . . . .	16
3.4	Precision testing . . . . .	18
3.5	Comparing experimental data and predictions . . . . .	21
3.6	Parameter selection . . . . .	23
3.7	Testing at Karolinska Universitetssjukhuset, Solna . . . . .	25
<b>4</b>	<b>Discussion</b>	<b>26</b>
4.1	Testing at Elekta Instrument AB . . . . .	26
4.1.1	Collimator choice . . . . .	26
4.1.2	Velocity testing . . . . .	27
4.1.3	Acquisition time testing . . . . .	27

4.1.4	Precision testing . . . . .	28
4.1.5	Comparing experimental data and predictions . . . . .	28
4.1.6	Parameter selection . . . . .	29
4.2	Testing at Karolinska Universitetssjukhuset, Solna . . . . .	30
4.3	Detection design improvements . . . . .	30
<b>5</b>	<b>Conclusion</b>	<b>32</b>
<b>A</b>	<b>State of the art</b>	<b>33</b>
A.1	Introduction to gamma radiation . . . . .	33
A.1.1	Radioactive decay . . . . .	33
A.1.2	Gamma radiation interaction with matter . . . . .	34
A.1.2.1	Photoelectric absorption . . . . .	34
A.1.2.2	Compton scattering . . . . .	35
A.1.2.3	Pair production . . . . .	36
A.1.2.4	Dominating interaction . . . . .	37
A.2	Leksell Gamma Knife® . . . . .	37
A.2.1	Placement of sources and collimators . . . . .	38
A.2.2	Movement of the patient . . . . .	40
A.3	Noise . . . . .	40
A.4	Setup for radiation detection . . . . .	41
A.4.1	Motor . . . . .	42
A.4.2	Detector types . . . . .	42
A.4.2.1	Scintillator with a photomultiplier tube . . . . .	42
A.4.2.2	Solid-state detector . . . . .	42
A.4.3	Electrometer . . . . .	43
A.4.3.1	PC Electrometer Software . . . . .	44
A.4.4	EtherCAT . . . . .	45
A.4.5	TwinCAT . . . . .	46
A.4.6	<sup>60</sup> Co setup for experiments . . . . .	46
A.4.7	Dose limit . . . . .	47
A.5	Radiation beam profile . . . . .	47
A.5.1	Inverse square law . . . . .	48
	<b>Bibliography</b>	<b>49</b>

# Chapter 1

## Introduction

There are parts of the body where surgical intervention is undesirable, and structures deep inside the brain are part of them. Lars Leksell, the founder of Elekta AB, developed the Leksell system primarily to tackle the issue of deep brain surgery. The Leksell system is a stereotactic system, which function is to locate deep structures, such as tumors, in the brain in relation to an external three dimensional frame, which at the same time works as a coordinate system [6].

After the development of the Leksell system, the treatment focus started to shift from surgical intervention towards non-invasive alternatives. This is where the Leksell Gamma Knife<sup>®</sup> (LGK) started being developed. The development started with ultrasound but was later on rejected due to low accuracy without opening the skull. Irradiation with protons was being considered and provided decent results but seemed too impractical for routine use because of the synchrocyclotron's large size. Later on the use of <sup>60</sup>Co sources was chosen since it provided acceptable results and was practical to use [6].

The LGK consists of either 192 or 201 <sup>60</sup>Co sources depending on the specific model. This thesis will solely focus on the LGK with 192 sources. At the time of inserting sources into the LGK, the sources are counted and confirmed to be the correct number. During recent years, multiple regulatory agencies have been asking for evidential proof and continuous determination of the number of sources in a LGK. The reason for this is the increased focus on security. Quality assurance and calculation tools exist and are used by employees at Elekta Instrument AB (Elekta). These tools can detect and measure the amount of radiation and therefore indirectly the number of sources. To en-

sure that all sources are located in the LGK, this thesis will focus on counting each of the sources separately to remove the influence of the other sources as well as directly detecting the position of the supposed missing  $^{60}\text{Co}$  source.

The use of the counting device proposed by this thesis would enable Elekta to provide direct information about the number of sources in a specific LGK in a short amount of time and therefore reassure the regulatory agencies that no  $^{60}\text{Co}$  sources are missing.

## 1.1 Goal of thesis

The purpose of this master thesis is to design and investigate if one can develop a fast and precise system to count all existing sources in an LGK. Apart from this, the thesis will focus on optimizing parameters in order to reduce the counting time.

# **Chapter 2**

## **Methods and materials**

### **2.1 Source detection system**

The system for  $^{60}\text{Co}$  source detection is composed of many components that can be divided into two main blocks. One block comprehends all necessary devices for detection of gamma radiation, the other block is the gantry for moving the detector. The two blocks are shown in Figure 2.1. A more full explanation of the components can be found in Section A.4.

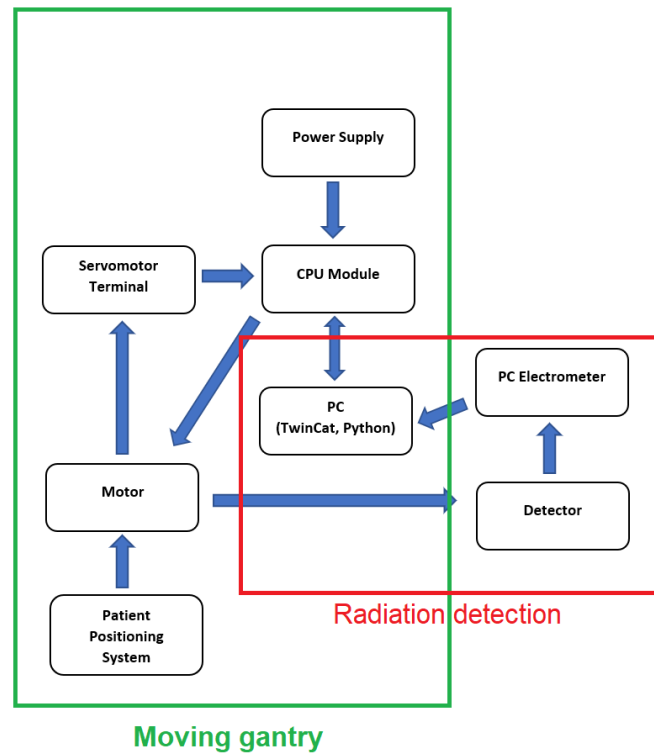


Figure 2.1: Block diagram showing all parts of the radiation detection block and the moving gantry block as well as their respective connection.

### 2.1.1 Radiation detection

The radiation detection block consists of a detector, an electrometer and the electrometer software.

- Detector

The detector used is a solid state detector from the company PTW (PTW 60016 Dosimetry Diode P), see Figure 2.2. It has the attributes shown in Table 2.1. To investigate if the detector could detect radiation or not, the detector was placed in front of one  $^{60}\text{Co}$  source. The output was registered using either an oscilloscope or an electrometer. The radiation was increased and decreased during this time, and if the detector output followed the curve of the radiation output the detector was deemed suitable.

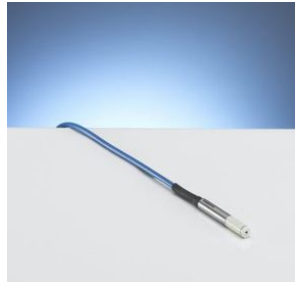


Figure 2.2: Dosimetry diode P from PTW used in detection measurements [15].

Table 2.1: Detector attributes

Detector	
Type	PTW 60016 Dosimetry Diode P
Material	Silicon
Energy response	9 nC/Gy
Sensitive area	1 mm <sup>2</sup> circular area, 30 $\mu$ m thick
Energy range	1.17 - 25 MeV

- Electrometer

The electrometer used was a PC electrometer from the company Sun Nuclear, where the detector previously mentioned is connected directly to it. The electrometer is then connected to a PC where the detector's output is visually presented in a software called PC Electrometer. The attributes of the electrometer is shown in the table below.

Table 2.2: Electrometer attributes

Electrometer	
Type	PC Electrometer
Charge range	2 pC – 10 mC
Acquisition time, lowest	25 ms
Connection	USB to PC
Resolution	15 fC

- PC Electrometer software

The PC Electrometer software is used in order to gather radiation data from the electrometer and therefore the detector. In the software the

acquisition time can be chosen to a lowest possible value of 25 ms, where the standard value is 500 ms.

### 2.1.2 Moving gantry

- Motor

The motor was used in order to move the detector, attached to a motor arm, in a circular motion. The motor is connected to a servomotor terminal, which sends information through a CPU module powered by a power supply. The specific motor has the characteristics in the table below.

Table 2.3: Motor attributes

Motor	
Type	AM8131 Servomotor
Torque	1.35 Nm
Connection	One cable technology
Shaft diameter	16 mm

- TwinCAT

In order to control the motors position and gather positional information of where the detector is located, TwinCAT was used. TwinCAT is a motor controlling software which performs those tasks.

## 2.2 Testing at Elekta Instrument AB

In this section I will describe the testing setup, as well as the tests performed at Elekta Instrument AB. The setup for doing experiments with a single  $^{60}\text{Co}$  source is shown in Figure 2.3 below.

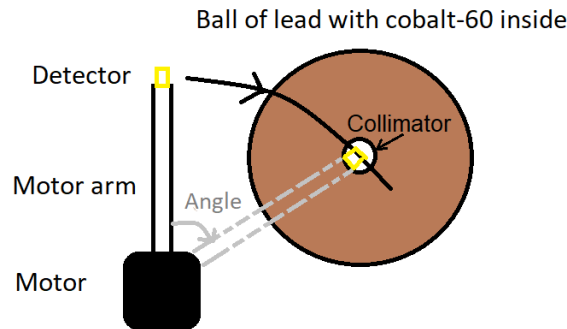


Figure 2.3: Testing setup for testing with one radioactive  $^{60}\text{Co}$  source. Motor with motor arm and detector attached is shown on the left, moving over the collimator opening where the source is located.

At the start of each test, the motor arm was placed in an upright position, set as  $0^\circ$ . The detector was then moved past the collimator opening, with a specified velocity and the electrometer output signal was acquired with a specified acquisition time. The velocity and acquisition time both depends on which test was performed. All the tests, except for the second precision test, were performed with this setup.

During the measurements, the PC Electrometer software exports the radiation data to a text file which is updated with new data every  $X$  seconds, where  $X$  is the chosen acquisition time.

Apart from this, correction for background radiation was obtained by acquiring data during 60 seconds with the detector positioned outside of the collimator opening. The mean value of this data was then subtracted from the electrometer output for all successive measurements.

### 2.2.1 Collimator testing

The collimator testing was performed in order to determine which collimator size provided the best result. Three different collimators were tested: 4mm, 8mm and 16mm in diameter. The tests were performed with a velocity of 0.03 degrees/s and an acquisition time of 0.5 s.

### 2.2.2 Velocity testing

The velocity testing was performed in order to determine how the angular velocity of the motor arm affected the electrometer output. The velocities tested were 0.03 degrees/s, 0.15 degrees/s, 0.6 degrees/s and 1.5 degrees/s. The tests were performed with a 8 mm collimator and an acquisition time of 0.5 s.

### 2.2.3 Acquisition time testing

The acquisition time testing was performed in order to determine how the acquisition time of the electrometer affects the electrometer output. The acquisition times tested were 0.5 s, 0.3 s, 0.1 s and 0.05 s. The tests were performed using a 8 mm collimator and a velocity of 0.03 degrees/s.

### 2.2.4 Precision testing

Two precision tests were performed in order to determine the source detection system's ability to provide the same result when performing a single test repeatedly.

1. Moving over the  $^{60}\text{Co}$  source multiple times using the same parameters:  
The electrometer output was recorded with an acquisition time of 0.5 s and a velocity of 1.5 degrees/s while moving over the  $^{60}\text{Co}$  source. This procedure was repeated 8 times.
2. Measuring electrometer output at different radiation intensities of the  $^{60}\text{Co}$  beam profile:  
The detector was placed at three different positions with different radiation intensity: outside the collimator opening, at the edge of the collimator opening and in the center of the collimator opening. For each position, the electrometer output was sampled every 0.5 s for 400 samples.

## 2.3 Parameter selection

After examining how different parameters affect the electrometer output, optimal parameters had to be chosen for testing on a LGK at Karolinska Universitetssjukhuset, Solna. This in order to reduce the counting time for the source detection system. Acquiring these optimal parameters would be very time-consuming in practice, therefore the tests were performed theoretically

instead.

To do this, the first step was to construct a radiation beam profile from the  $^{60}\text{Co}$  source at Elekta Instrument AB, such as the one explained in Section A.5. This was done through the use of the testing setup shown in Figure 2.3, and the parameter values used was an 8 mm collimator, a velocity of 0.03 degrees/s and an acquisition time of 0.5 s. The result of this is a plot of electrometer output as a function of the motors angular position, see angle in Figure 2.3. By applying this beam profile to all of the LGKs 192 sources, a representation of the radiation output from the LGK (when using the source detection system) was obtained. This was visualized in a graph with the electrometer output as a function of the sources angular position, with one beam profile for each source, shown as the blue line in Figure 3.13. This is what was used for the parameter selection.

Before the parameter selection could begin, the representation needed to be validated to respond to changes in parameter values equally as the source detection system. This was done by recreating the previous tests for velocity and acquisition time (see Section 2.2.2 and 2.2.3), and then comparing the results.

When the representation was validated to be able to represent the source detection system, the values for velocity and acquisition time could be optimized. A threshold was set in order to determine if a source would count as detected or not. The limit of the threshold was based on the results from Section 2.2.4. The parameter selection was performed through several trial and error tests, where the velocity was increased until not all sources were detected. Then, the acquisition time was lowered until all sources were detected and then the velocity was increased further. This was performed iteratively until the highest velocity was achieved while still detecting all sources, thus achieving the shortest detection time.

To compensate for the shift in position that occurred when changing the velocity and acquisition time, see Section 3.2 and 3.3, the following equation was used:

$$p = p_0 - 2vt \quad (2.1)$$

, where  $p$  is the corrected position and  $p_0$  is the original position.

## 2.4 Testing at Karolinska Universitetssjukhuset, Solna

### 2.4.1 Calculating coordinates for calibration

When testing at Karolinska, the source detection system was fastened to the head frame of the treatment bed. In order to have the motor centered in the LGK, a CBCT (Cone Beam CT) image of the source detection system was taken to gather the motor axis' position in the coordinate system of the LGK. The CT determination of the position is shown in Figure 2.4. When performing the test at Karolinska, the motor axis was moved to origo in the LGK's coordinate system based on the position previously provided.

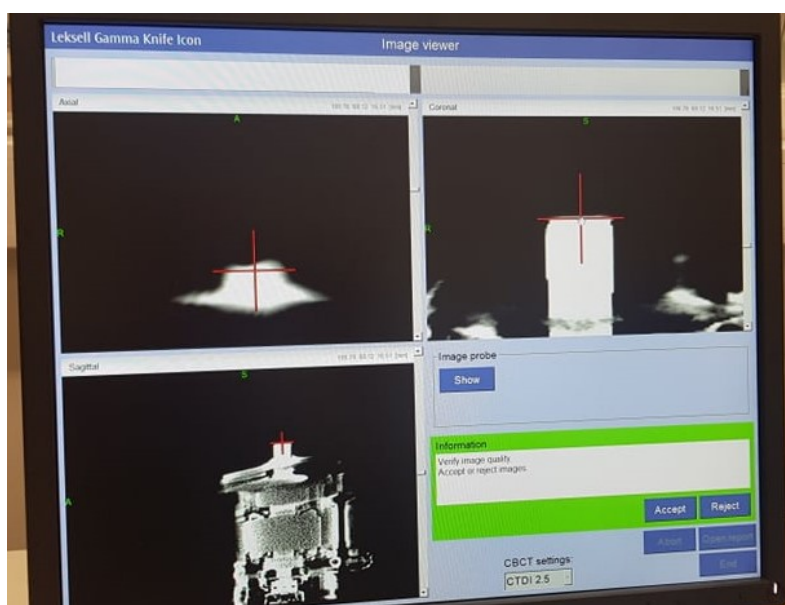


Figure 2.4: Calculating the position of the motor axis in the LGK coordinate system in three dimensions using a CBCT image.

The final test was performed at Karolinska Universitetssjukhuset, Solna with an LGK fully loaded with  $^{60}\text{Co}$  sources. The setup should not only be able to detect  $^{60}\text{Co}$  sources but have the ability to detect if a source does not exist. In order to detect that no source exist we need to remove some sources. This can only be done by closing off a full sector in the LGK, further explained in Section A.2.1. In the test, sector 4 was closed. The test was performed by using an 8 mm collimator, a velocity of 3.75 degrees/s and an acquisition time of 0.2 s. The detector was moved in the X-Y plane with the moving gantry and



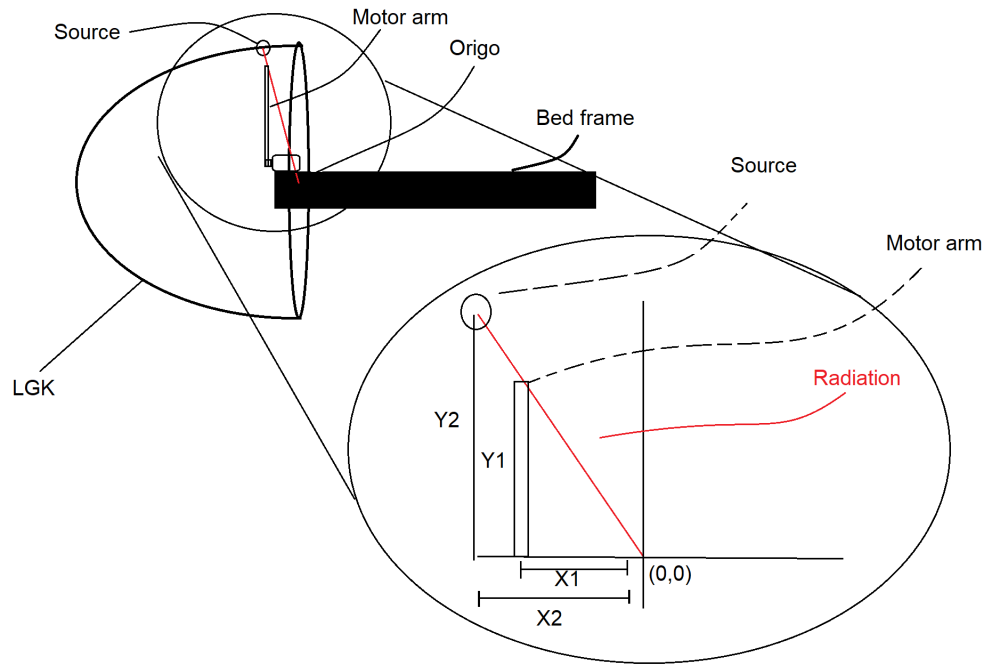


Figure 2.6: Motor arm position calculation

Using the PPS the source detection system needs to move to specific Z-coordinates for each of the source rings. These positions are illustrated in Figure 2.6 and are calculated by this formula:

$$X1 = \frac{X2 \cdot Y1}{Y2} \quad (2.2)$$

, where X1 is the calculated position of the motor axis and (X1, Y1, Y2) are known values.

- X2 Ring position from origo
- Y1 Motor arm length
- Y2 Collimator body distance, shown in Figure 2.5

# Chapter 3

## Results

The results after testing the setup as well as the parameter selection is presented down below in multiple plots. All the different tests are explained previously in Section 2.2.

### 3.1 Collimator testing

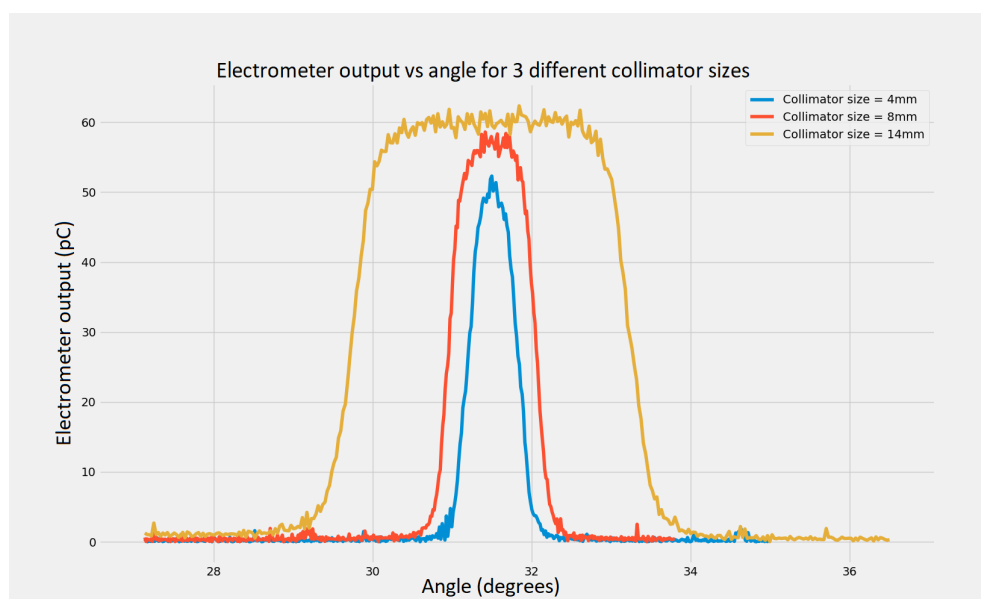


Figure 3.1: Electrometer output as a function of angular position for three different collimators.

In Figure 3.1 the electrometer output for different collimators as a function of detector angular position is shown. In all cases the velocity of the detector was 0.03 degrees/s and the detector acquisition time was 0.5 s.

## 3.2 Velocity testing

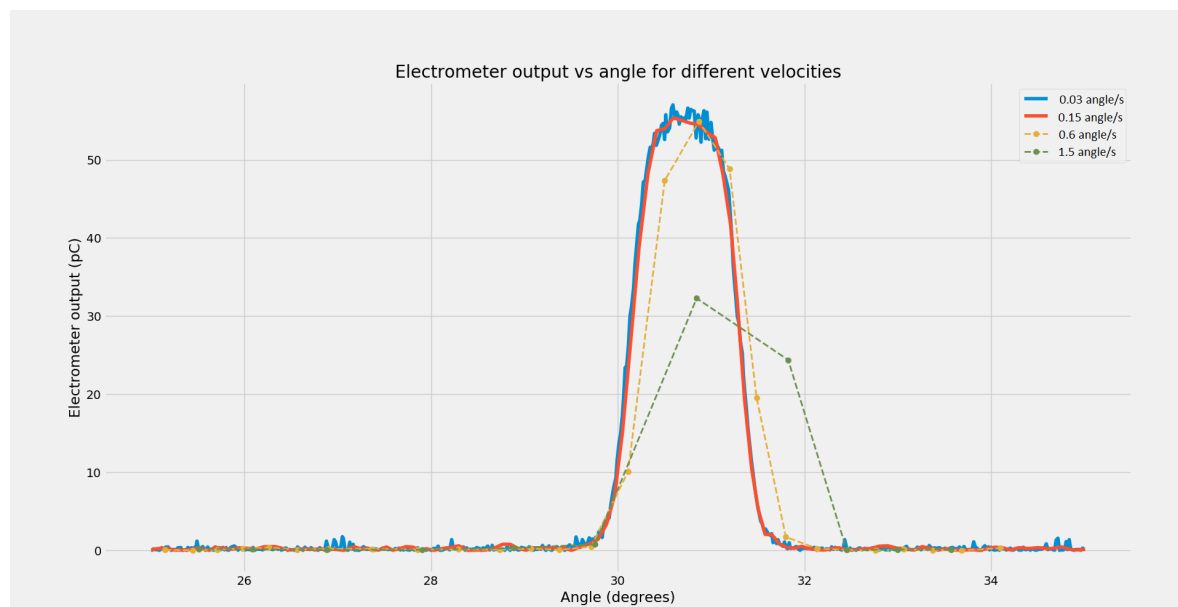


Figure 3.2: Electrometer output as a function of angular position for four different velocities using a 8 mm collimator and an acquisition time of 0.5 s.

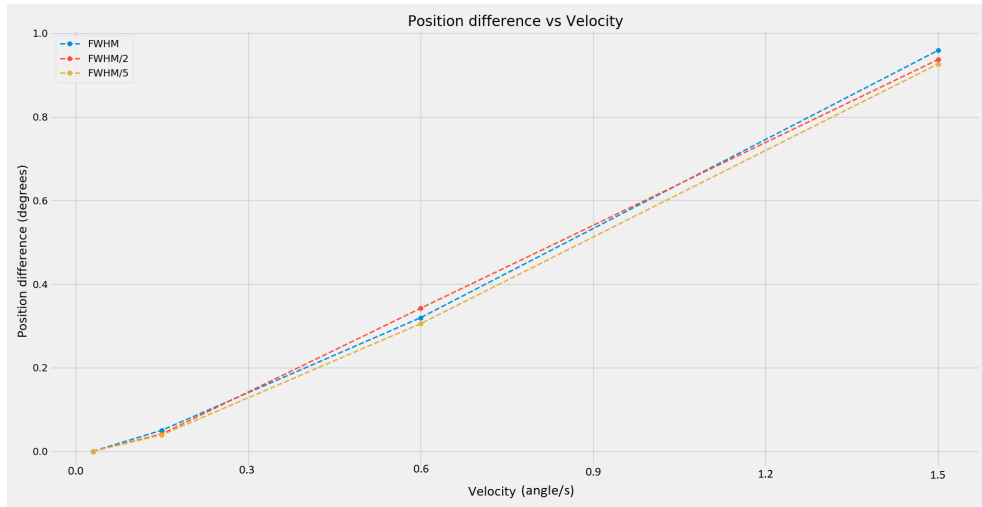


Figure 3.3: Peak position shift in Figure 3.2 as a function of angular velocity. The peaks were calculated through FWHM (Full Width Half Maximum) and the shift is in relation to the peak provided when using a velocity of 0.03 degrees/s.

In Figure 3.2 the results of our measurements with different angular velocities are shown. When increasing the velocity, there is a decrease in the electrometer output (peak value). The decrease is small at first but increases significantly at higher velocities. Apart from this the peaks are also shifted in the direction of movement of the detector, as shown in Figure 3.3. In other words, the peaks move to the right in the graph in Figure 3.2 as the velocity increases. Figure 3.2 also shows that the number of data points obtained during one full rotation decrease as the velocity increases.

### 3.3 Acquisition time testing

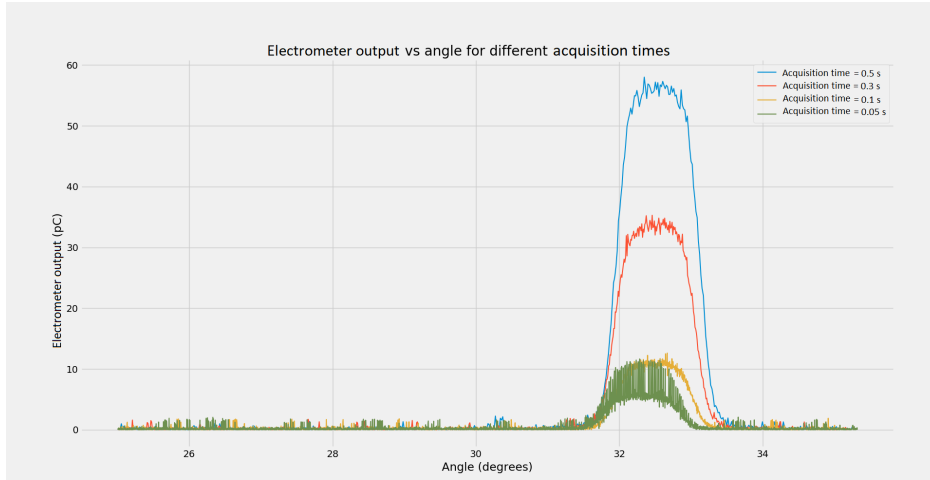


Figure 3.4: Electrometer output as a function of angular position for different acquisition times using a 8 mm collimator and a velocity of 0.03 degrees/s.

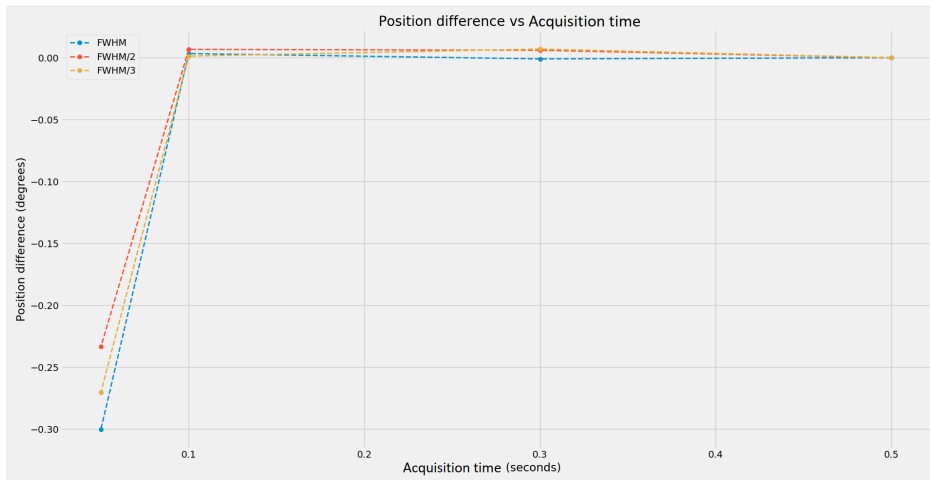


Figure 3.5: Peak position shift in Figure 3.4 as a function of the acquisition time, using a 8 mm collimator. The peaks were calculated through FWHM (Full Width Half Maximum) and the shift is in relation to the peak provided when using an acquisition time of 0.5 s.

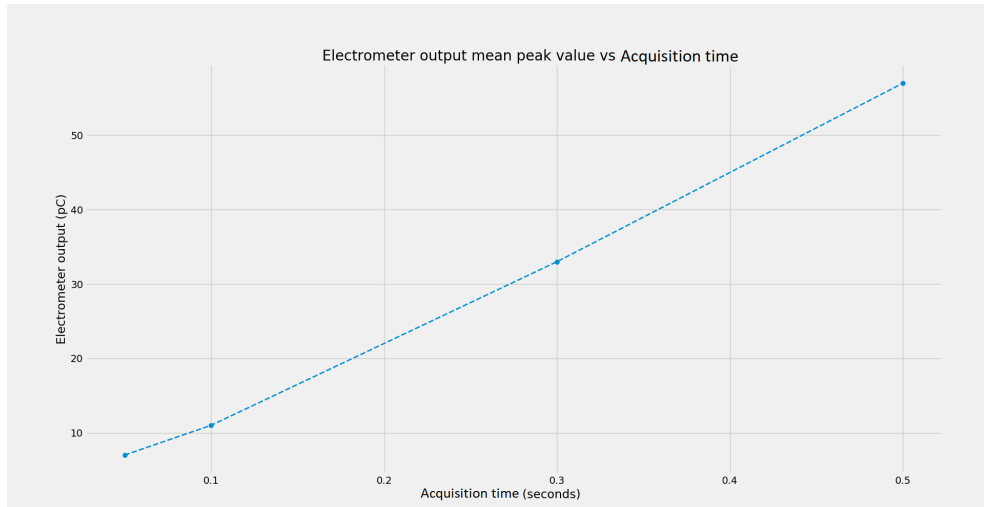


Figure 3.6: Electrometer output's mean peak value as a function of the acquisition time.

Figure 3.4 shows how the acquisition time affects the electrometer output. When the acquisition time decreases, there is a decrease in the electrometer output peak value, shown in Figure 3.6, and an increase in the noise level. The increase of the noise level can be observed by comparing the yellow data line with the green data line in Figure 3.4. Apart from this, increasing the acquisition time also causes a shift to the right, see the blue data line. This positional difference is shown in Figure 3.5, where the difference is close to zero unless the data acquisition time is very low.

### 3.4 Precision testing

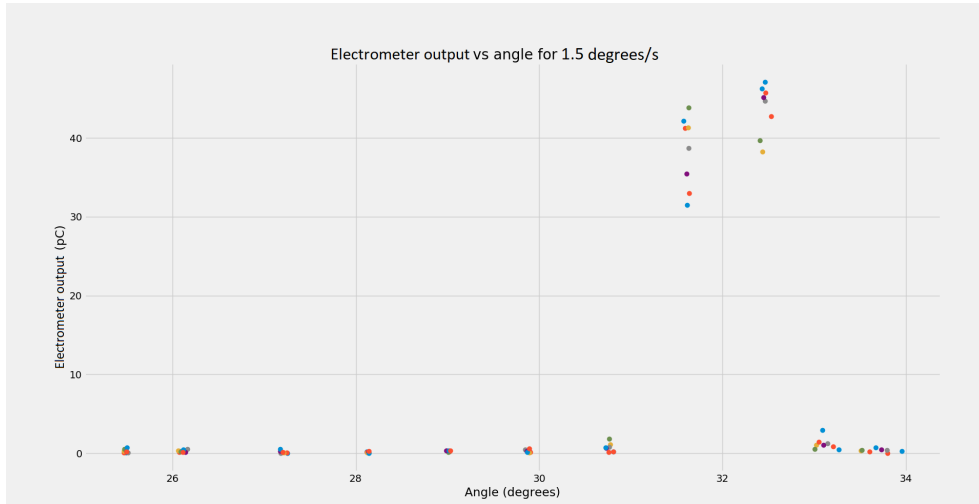


Figure 3.7: Electrometer output as a function of angular position, using a velocity of 1.5 degrees/s, an acquisition time of 0.5 s and a 8 mm collimator. Each colored point represents a different measurement (8 in total).

In Figure 3.7 the result of repeated measurements of electrometer output as a function of angular position is shown. All the measurements were performed using a velocity of 1.5 degrees/s, an acquisition time of 0.5 s and a 8 mm collimator.

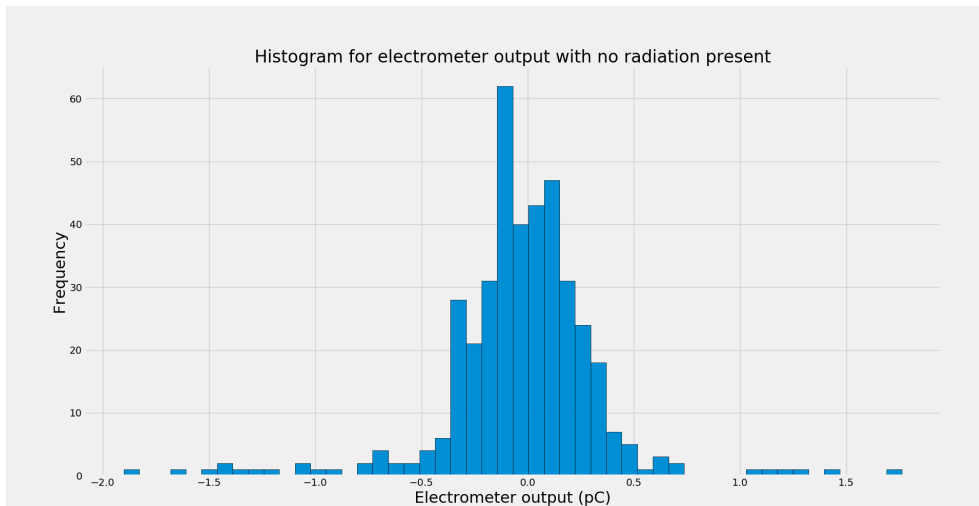


Figure 3.8: Histogram of electrometer output with no radiation present, total of 400 data points.

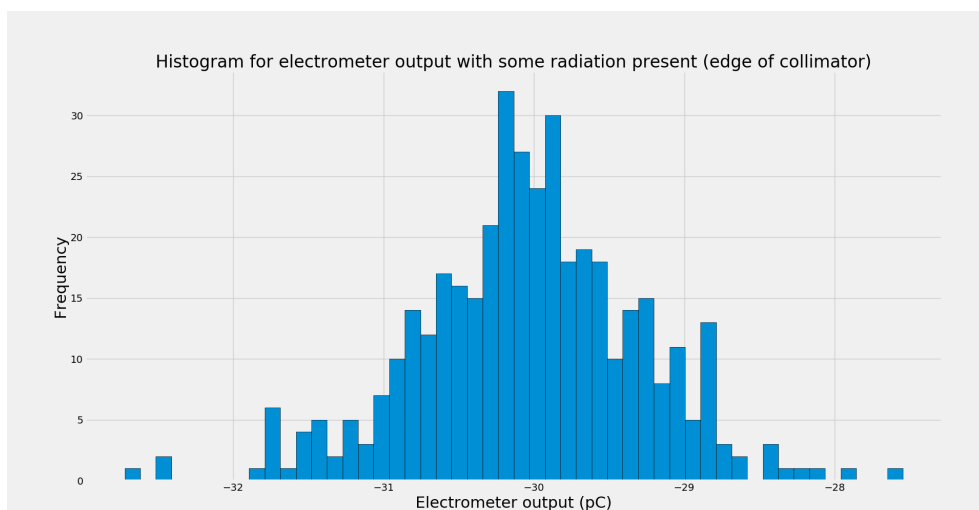


Figure 3.9: Histogram of electrometer output with some radiation present, total of 400 data points.

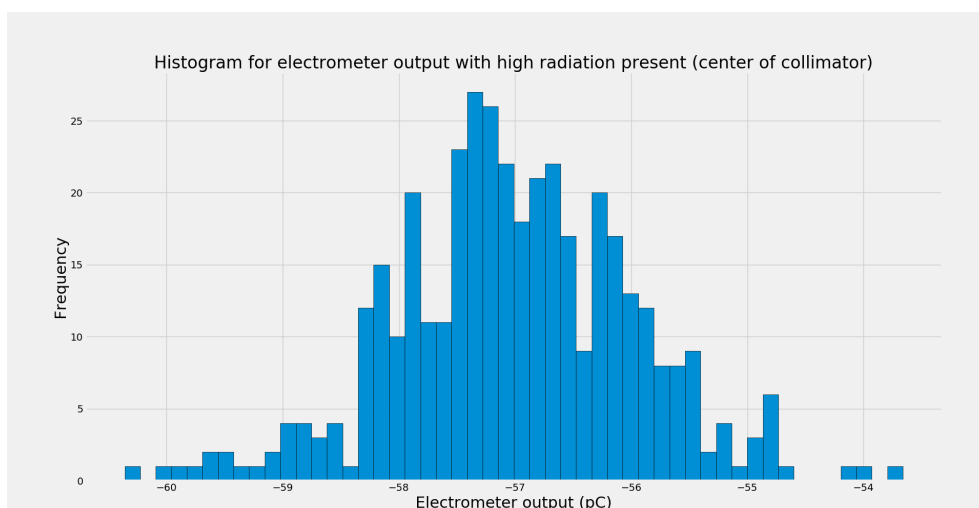


Figure 3.10: Histogram of electrometer output with high radiation present, total of 400 data points.

Table 3.1: Table showing the mean electrometer output and standard deviation for Figure 3.8, 3.9 and 3.10

	<b>Mean electrometer output with standard deviation</b>
No radiation	$0.0 \pm 0.4$ pC
Some radiation	$30.0 \pm 0.7$ pC
High radiation	$57 \pm 1$ pC

In Figure 3.8, 3.9 and 3.10 the distribution of the electrometer output when stationary at a specific motor position is shown. The different positions were: outside the collimator (no radiation), at the edge of the collimator opening (some radiation) and in the center of the collimator opening (high radiation). For each position, the electrometer output was sampled every 0.5 seconds for 400 samples. The mean electrometer output and their standard deviations for all three positions is shown in Table 3.1.

### 3.5 Comparing experimental data and predictions

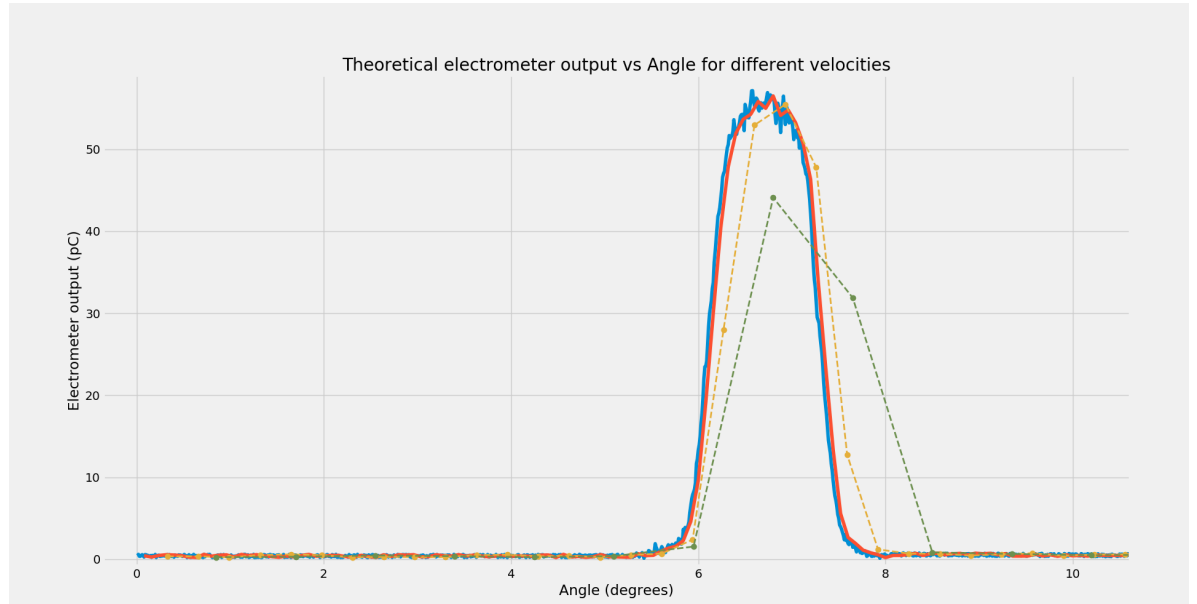


Figure 3.11: Theoretical electrometer output as a function of angular position for different velocities using a 8 mm collimator. Blue - 0.03 degrees/s, Red - 0.15 degrees/s, Yellow - 0.6 degrees/s and Green - 1.5 degrees/s.

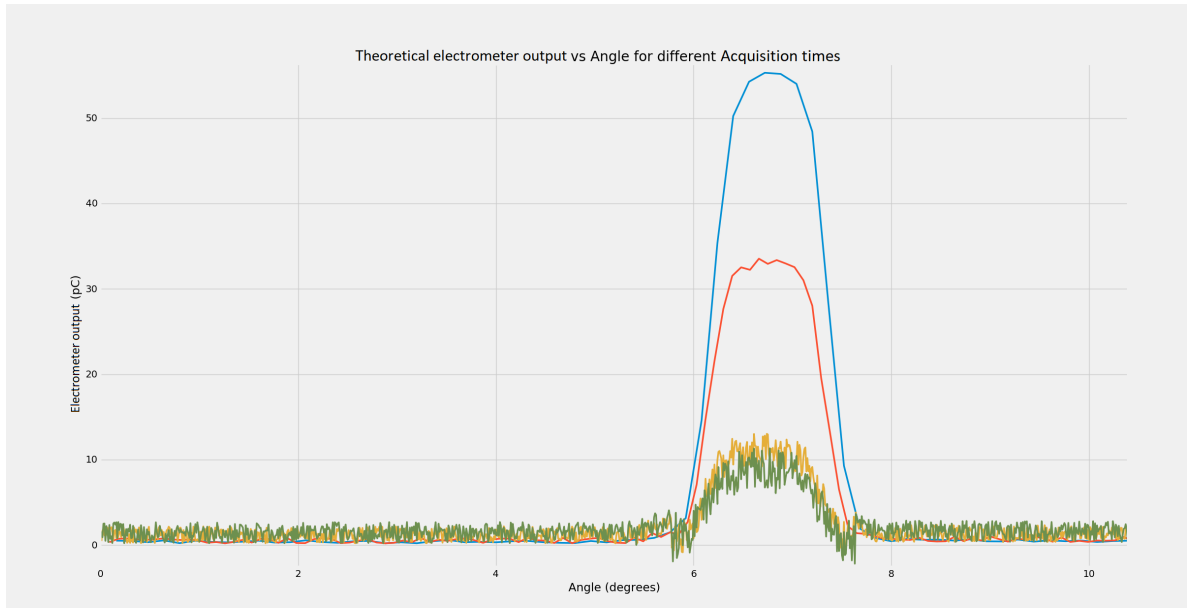


Figure 3.12: Theoretical electrometer output as a function of angular position for different acquisition times using a 8 mm collimator. Blue - 0.5 s, Red - 0.3 s, Yellow - 0.1 s and Green - 0.05 s.

In Figure 3.11 and 3.12, theoretical representations of the tests performed in Section 3.2 and 3.4 are shown. The test in Figure 3.11 can be compared to the test in Figure 3.2 and the test in Figure 3.12 can be compared to the test in Figure 3.4.

### 3.6 Parameter selection

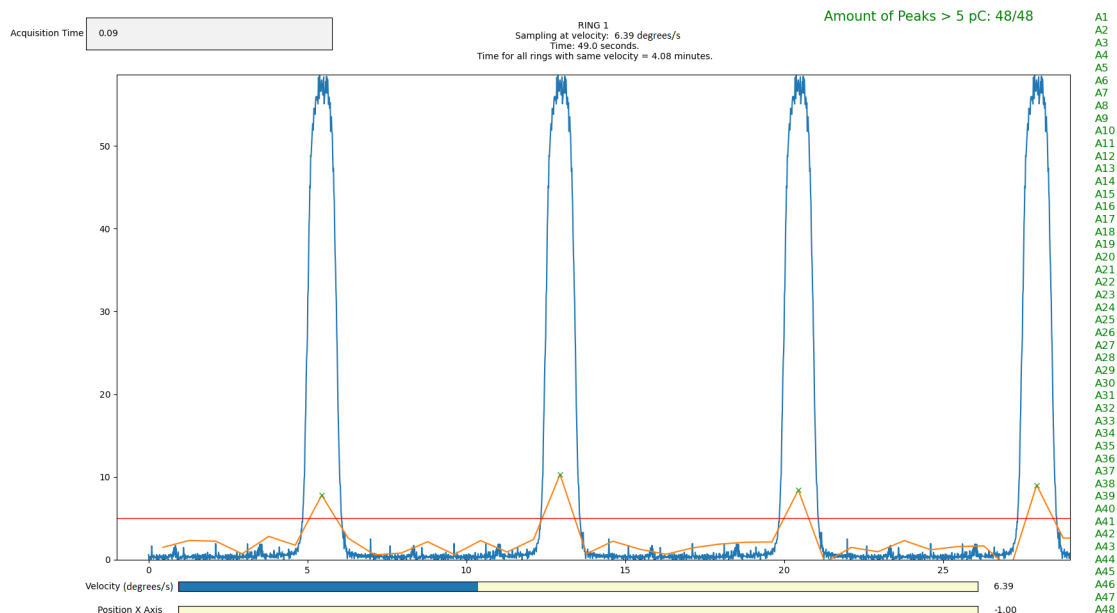


Figure 3.13: Electrometer output as a function of angular position using a velocity of 6.39 degrees/s, an acquisition time of 0.09 s and a 8 mm collimator.

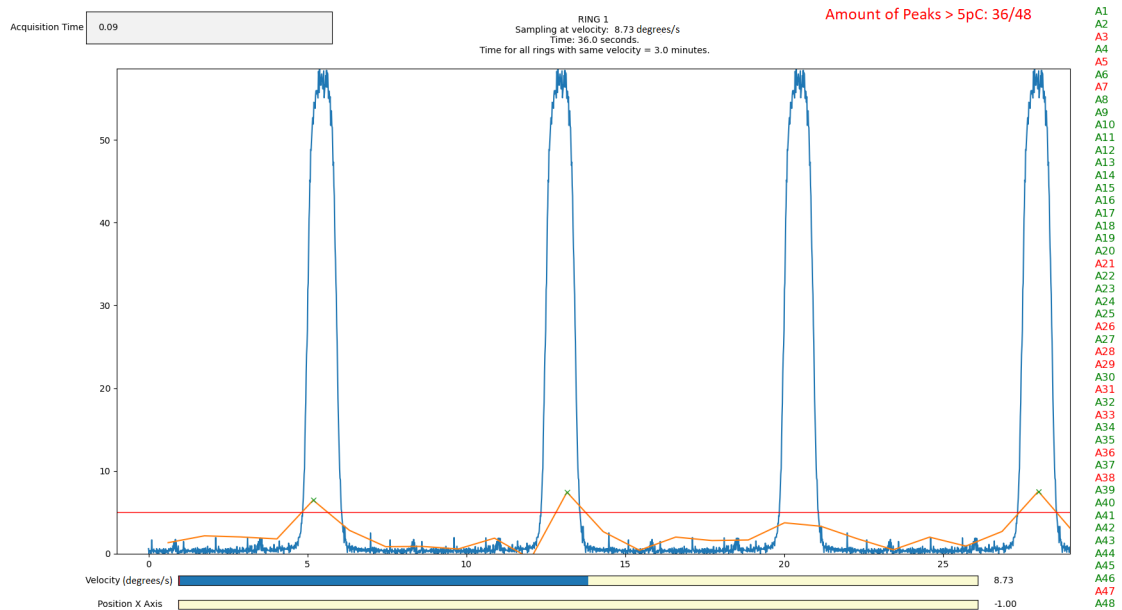


Figure 3.14: Electrometer output as a function of the angular position using a velocity of 8.73 degrees/s, an acquisition time of 0.09 s and a 8 mm collimator.

In Figure 3.13 and 3.14 the expected electrometer output as a function of the angular position using different parameter values are shown. The blue line represents the electrometer output from each source, and the orange line represents the output with the entered parameters. In the top left corner of the images, the desired acquisition time is entered, and to the right the list of sources are displayed. A green colored source means that it is detected and therefore meet the criteria of detection, otherwise it is displayed in red. The criteria of detection is also shown in the top right corner.

Figure 3.13 displays the expected electrometer output with optimized parameters. All the sources are still detected, as shown to the right in the image, but the total time of one revolution is decreased.

Figure 3.14 displays the expected electrometer output with non-optimized parameters. The velocity was increased until 10 or more sources were not detected because the sources electrometer output was below the threshold. This is shown to the right in the image where some sources are displayed in red instead of green, and the peaks are below the threshold.

### 3.7 Testing at Karolinska Universitetssjukhuset, Solna

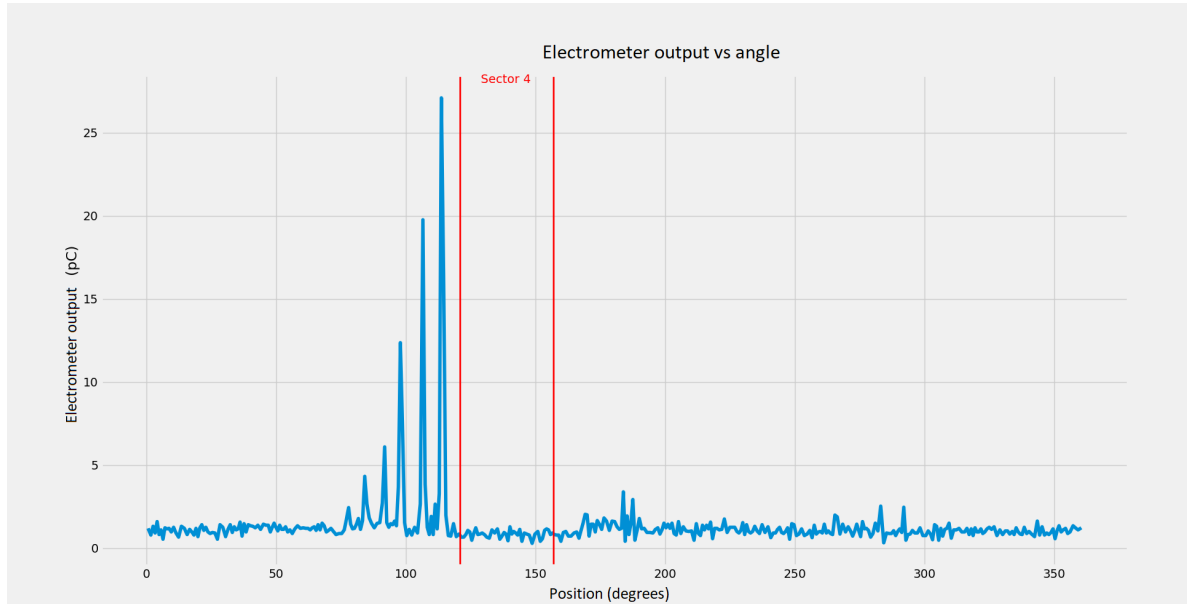


Figure 3.15: Results after testing at Karolinska Universitetssjukhuset, Solna. Electrometer radiation as a function of angular position using a velocity of 3.75 degrees/s, an acquisition time of 0.2 s and a 8 mm collimator.

The results shown in Figure 3.15 is gathered from testing at an LGK at KS. The radiation data is gathered from the 8 mm collimator in the first ring, velocity is 3.75 degrees/s and the acquisition time is 0.2 s. There are 6 peaks increasing in amplitude with increasing position to a maximum peak of 27.1 pC. The red lines show the values corresponding to sector 4, which is closed off, and no significant radiation is emitted from those collimators.

# Chapter 4

## Discussion

In this discussion I will explain the reasoning behind the choices made in this thesis, and also discuss the results from the testing in order to answer if the design constructed has the possibility to detect all sources in an LGK in a low amount of time. I will also discuss what could have been done differently to possibly improve the performance.

### 4.1 Testing at Elekta Instrument AB

#### 4.1.1 Collimator choice

For the testing at Elekta Instrument AB, the largest available collimator was chosen, which was an 8 mm collimator. The reason we wanted as big of a collimator as possible was due to the fact that a larger collimator leads to a larger beam profile, see Figure 3.1. This means that when moving over a source, a larger collimator provides more samples than a smaller collimator. This makes the sources easier to detect in a XY-plane and also in Z-direction, for coordinate system see Figure A.7. Apart from this, the larger amount of samples makes the resulting beam profile detected more representative of the sources original beam profile. In Figure 3.1, you can see that a 14 mm collimator was investigated as well. The reason for not using that collimator in the source detection system was that it was not available for long term use at Elekta Instrument AB. Additionally, the 8 mm collimator was more than sufficient since the detector of the system is relatively small. Therefore increasing the collimator size further would result in a loss of spatial resolution.

### 4.1.2 Velocity testing

When observing the graph in Figure 3.2 we can see how the velocity affects the results of the radiation output. An increased velocity both decreases the peak value and shifts the peak in the direction of movement of the detector, which can be seen in Figure 3.3. This shows that in order to detect all sources, you can only increase the velocity to a certain degree without also decreasing the acquisition time. The reason for this is that an increased velocity with the same acquisition time results in fewer samples, which leads to a decreased peak intensity. When increasing the velocity too much, the peak will not be distinguishable compared to the noise.

The shift that occurs is also due to the fact that a higher velocity results in a lower amount of samples. Each sample will then take up a larger amount of the whole measurement, and the signal from each sample is displayed at the end of acquisition time. To make sure that the position of the source is acquired correctly, the shift is compensated using the formula described in Equation 2.1.

### 4.1.3 Acquisition time testing

Observing Figure 3.4 you can see that an increased acquisition time increases the peak value and shifts the peak in the direction of the movement of the detector. You can also see that a decreased acquisition time results in an increased noise. The reason for the increased peak value is that the longer the acquisition time, the more gathered signal. In Figure 3.6 you can see that the electrometer output decreases linearly when decreasing the acquisition time. The peak shift occurs for the same reason as described above under Section 4.1.2. In Figure 3.5 you can see that the peak position shift increases with an increased acquisition time. It seems that the shift only happens up to an acquisition time of 0.1 s. However, increasing the acquisition time more dramatically than this should continue to shift the peak position. Just as with the velocity, the shift is compensated for using the formula described in Equation 2.1.

The reason for the increasing of the noise when decreasing the acquisition time could be because of internal noise in the electrometer. Otherwise it could be because of the signal being gathered over a smaller time frame, which would be easily influenced by inconsistencies in the signal.

#### 4.1.4 Precision testing

From Figure 3.7 we observe that the precision of the signal is not ideal. When performing the same tests multiple times the results are inconsistent. However, this is expected since the setup of the source detection system is not perfectly stable, which can cause inconsistencies in the motors movement. Apart from this, there is a difference in the amount of photons hitting and depositing their energy in the detector at each different measurement. This follows a Poisson distribution and can be seen in Figures 3.9 and 3.10. In Table 3.1, we can observe that the variation in signal decreases with increasing electrometer output. This is to my advantage since the source detection system is created to detect high radiation.

Figure 3.7 also shows that the positions become less precise towards the end of the measurement, which is when the motor is coming to a halt. This is likely because the motor is breaking differently or at different times at each measurement. To prevent this issue when calculating all sources, the motor should move  $>360^\circ$  so that this breaking inconsistency does not affect the data.

#### 4.1.5 Comparing experimental data and predictions

By comparing Figure 3.2 and Figure 3.11 we can observe a lot of similarities. When velocities are low, as shown in both figures in colors blue, red and yellow, the graphs are very similar. When the velocities increase, as shown with the color green in the figures, the data lines are not as similar. This is because of the results shown in Figure 3.7. When the velocity is 1.5 degrees/s there exist a lot of variation in the signal output. This could provide the difference in the two different graphs. When comparing Figure 3.4 to Figure 3.12, you can see that these are also very similar.

These results shows that the parameter selection could be performed with the current representation and knowledge of the  $^{60}\text{Co}$  source at Elekta. However, there are two aspects that were not accounted for that could affect parameter selection. Firstly, it is the difference in activity between the  $^{60}\text{Co}$  source at Elekta and the LGKs sources at Karolinska Universitetssjukhuset. The source available for testing at Elekta is around 7 years old at the time of testing, which means that its activity is about 60% of a new  $^{60}\text{Co}$  source. The sources in the LGK at Karolinska is replaced more frequently, which means they have a higher activity. Taking the activity into consideration would enable the parameters to be selected for a lower total detection time. However the activity

of the sources at Karolinska was not known previous to the test. Additionally, the activity of the sources is different in every LGK, and we did not know which LGK we were going to be able to test on. This issue could be solved by having the source detection system gather the activity of one sources in the LGK on the day of testing at Karolinska, and then select the parameters based on the gathered activity. This would however require the parameter selection to be performed automatically instead of manually since the time for testing at Karolinska was very limited. Any such automatic parameter selection was not created and tested with.

Secondly, there is a big difference in the number of sources present at the different testings. The testing before Karolinska was performed on one source only, but in an LGK there are 192 sources. This high number of sources increases the risk of noise in our detector due to Compton scattering. The noise present while testing at Elekta can be seen in Figure 3.8, which is centered around 0 pC. In an LGK, this number would be higher, and this difference was not accounted for due to not using an automatic parameter selection.

#### 4.1.6 Parameter selection

In order to detect all active  $^{60}\text{Co}$  sources in an LGK in as low time as possible, velocity and acquisition time needed to be selected for the lowest total detection time. Figure 3.13 and Figure 3.14 shows the result of a measurement with optimized and non-optimized parameters. You can see that measurement in Figure 3.13 is optimized since all sources are detected, but they are still just above the threshold. This means that no time is wasted and the measurement is as short as possible. This Figure also contains the result of the parameter selection, i.e. the optimal parameters for detection. In Figure 3.14 the parameters are not optimized, causing not all sources to be detected. The third source in the image is below the threshold, and therefore could just as easily be noise. Another version of a measurement with non-optimized parameters would be with the peaks being far over the threshold, which means that the measurement took longer than it had to. The parameters could have been selected for a lower detection time if more time had been put into setting the threshold. A lower threshold while still only detecting the sources would mean that the measurement time was reduced.

As mentioned previously, this parameter selection was performed through trial and error. This could have been done automatically instead, which would have

been less time consuming and made it easier to find optimal parameters for different LGKs.

## 4.2 Testing at Karolinska Universitetssjukhuset, Solna

We only had time to perform one test at the day of testing at Karolinska. Therefore, it was decided to close of one sector (sector 4) to see if the source detection system could not only detect existing sources, but also detect that the sources in sector 4 were missing.

As seen in Figure 3.15 a minority of the total amount of sources were detected. During this test, 48 sources should be detected. When studying the Figure, you can see that only about 6 sources were detected, represented by the peaks in the graph. These sources also increase in amplitude until we reach sector 4, represented by the two red lines in the figure. The reason for this could be due to the fact that the motor setup was not perfectly aligned with the XY-plane in the LGK, see Figure A.7. In that case, the detector will cut through the XY-plane instead of following it. Then only a few sources would be detected, and with different intensities since the distance to them varied. However, we can see that all the sources in sector 4 were correctly detected as missing in Figure 3.15. Solving this issue could be done by 3D printing a holder for the motor to the head frame of the patient bed. Apart from this, having a motor arm 3D printed specifically for the chosen detector would enable the motor arm to move more stable as well as having the detector less provisionally positioned.

## 4.3 Detection design improvements

As mentioned earlier, there are some possible potential areas of improvement. One area that I have not discussed yet is improvements of the detection design. The detection could be improved in two different ways: using multiple detectors or using a larger detector.

The use of more than one detector could significantly reduce the total time for detecting all sources in an LGK. If the detectors are arranged evenly in 360 degrees around the LGK ring, then each individual detector would cover its own portion of the ring. For each added detector the total detection time should be reduced since the motor does not need to move a full 360 degrees.

One issue with this solution is the cost of all of the detectors. The increase in cost might not be worth the decrease in detection time. Another issue is that multiple detectors would increase the size of the source detection system, because of multiple motor arms. A larger sized system might lead to compatibility and setup difficulties at the hospital.

Using a larger detector, perhaps a curved detector, could be used to detect multiple sources at the same time. By detecting multiple sources, more signal is detected with every acquisition time. This would mean the velocity could be increased which would reduce the total detection time. One issue with this could be if a source is missing, the detection system would not be able to identify the position of that specific source. A possible solution could be to run the detection again but at a slower velocity to determine where the missing source is located.

# Chapter 5

## Conclusion

The goal for this thesis was to determine if one could develop a fast and precise system to count all existing sources in a Leksell Gamma Knife<sup>®</sup>", and to this as time efficient as possible. Improvements to the design is needed in order for the system to have better stability in order to detect all sources in an LGK and not just some of them. The parameter selection could be improved by automating the parameter selection, thus being able to adapt the detection for each individual LGK. My conclusion is that I produced a system which could detect <sup>60</sup>Co sources in an LGK, but the design could be improved for better stability.

# Appendix A

## State of the art

### A.1 Introduction to gamma radiation

#### A.1.1 Radioactive decay

Radioactive decay is the process when an atomic nucleus emits energy and particles spontaneously. When this occurs, the nucleus is said to be unstable and radioactive. The parent element will undergo a transformation into a daughter element, releasing particles and radiation, such as gamma rays in the process.

Multiple categories of radioactive decay exist, but this part will solely focus on  $\beta^-$ -decay since it is the radioactive decay of  $^{60}\text{Co}$ , the source used in the measurements in this thesis. In the decay of  $\beta^-$  a neutron is transformed into a proton which ejects a negatively charged electron, as well as an antineutrino particle, which is a neutral particle with small mass. The decay of  $^{60}\text{Co}$  is written as follows:



Cobalt therefore decays to nickel, an electron and an antineutrino particle [12]. The nickel produced is in an excited state and due to the excitation, the nickel will later decay through the emission of gamma rays [11]. For  $^{60}\text{Co}$  the emitted gamma rays have the energy of 1.17 MeV and 1.33 MeV as seen in the decay scheme in Figure A.1. The energy released corresponds to the mass difference between cobalt and nickel.

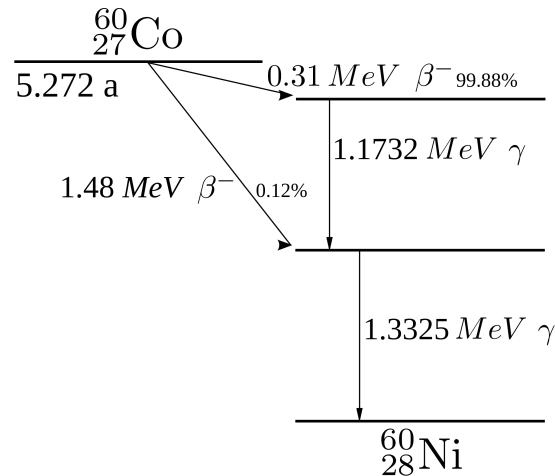


Figure A.1: Decay scheme of  $^{60}\text{Co}$ . Arrows indicating the decay path as well as the energies released. The percentages shows the occurrence ratio<sup>1</sup>.

## A.1.2 Gamma radiation interaction with matter

When gamma rays are emitted from the decay of  $^{60}\text{Co}$ , the radiation may interact with matter. This could occur in several possible ways. For  $^{60}\text{Co}$  three main kinds of interactions exist, photoelectric absorption, Compton scattering and pair production. All of these interactions will lead to a partial or absolute transfer of the particle's energy to the matter [11].

### A.1.2.1 Photoelectric absorption

In the process of photoelectric absorption, a photon interacts with an atom which absorbs the energy of the photon and the photon completely disappears. That causes an energetic electron, usually labeled as photoelectron, to be ejected from one of the atom's inner electron shells. For gamma rays of sufficient energy the interaction usually occurs at the K-shell of the atom, as seen in Figure A.2(a).

<sup>1</sup>[https://commons.wikimedia.org/wiki/File:Cobalt-60\\_Decay\\_Schemep.svg](https://commons.wikimedia.org/wiki/File:Cobalt-60_Decay_Schemep.svg)

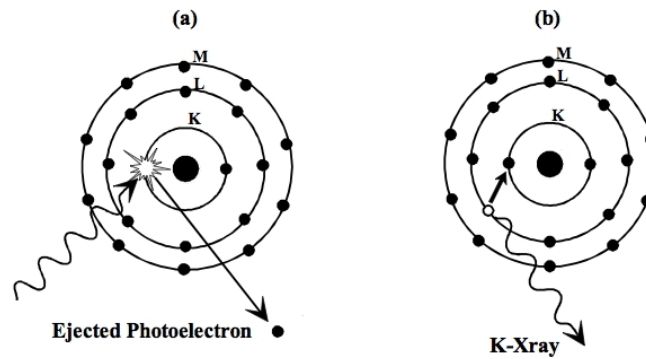


Figure A.2: The Photoelectric Effect - electron ejection (a) and fluorescent X-ray emission (b)<sup>2</sup>.

This interaction leaves a vacancy in the K-shell of the atom which will be filled by electrons in other shells, this could lead to a release of a characteristic X-ray, as seen in Figure A.2(b). The characteristic X-ray will usually be absorbed by photoelectric absorption with less bound shells [11].

The energy for the ejected photoelectron  $E_{e^-}$  is determined by Equation A.1 [11]:

$$E_{e^-} = h\nu - E_b \quad [\text{J}] \quad (\text{A.1})$$

, where  $h\nu$  is the energy of the incoming photon.

- $h$  Plancks constant
- $\nu$  photon frequency
- $E_b$  binding energy of photoelectron

#### A.1.2.2 Compton scattering

Compton scattering is the process where a gamma photon interacts with an electron in the material. The incoming gamma photon interacts with an electron and is scattered with an angle  $\theta$  with respect to its original direction (see Figure A.3(a)).

<sup>2</sup><https://commons.wikimedia.org/wiki/File:PhotoelectricEffect.jpg>

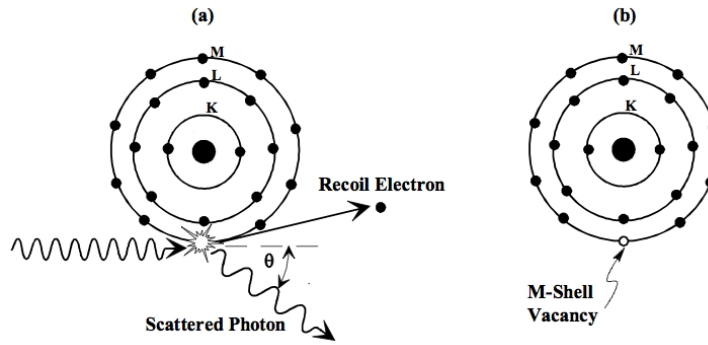


Figure A.3: The Compton Effect - (a) photon scattering and electron ejection leading to (b) an ionized atom<sup>3</sup>.

The photon transfers part of its energy to the electron, furthermore described as a recoil electron. The portion of the energy transferred to the recoil electron is dependent on the scattering angle  $\theta$ . Where a larger scattering angle corresponds to a lower energy transfer to the electron [11].

The energy of the recoil electron  $h\nu'$  is determined by Equation A.2:

$$h\nu' = - \frac{h\nu}{1 + \frac{h\nu}{m_0c^2}(1 - \cos(\theta))} \quad [\text{J}] \quad (\text{A.2})$$

, where  $m_0c^2$  is the rest mass energy of an electron and  $h\nu$  is the energy of the incoming photon [11].

- $h$  Plancks constant
- $\nu$  photon frequency
- $m_0$  mass of electron
- $c$  speed of light
- $\theta$  scattering angle

### A.1.2.3 Pair production

If the energy of the gamma photons emitted from the radioactive decay exceed twice the rest energy of an electron, therefore over 1.02 MeV, then pair production is a possibility. In this interaction, which must occur in the Coulomb field of the nucleus, the interacting photon completely disappears and is instead replaced by an electron-positron pair. All the energy above the necessary 1.02

<sup>3</sup><https://commons.wikimedia.org/wiki/File:ComptonEffect.jpg>

MeV is converted into kinetic energy divided between the electron and the positron. The probability of pair production interactions rises with increasing energy [11].

#### A.1.2.4 Dominating interaction

Depending on the energy of the incoming gamma rays and the atomic number of the interacting material, different interactions with matter dominate. As shown in Figure A.4, independent of the interacting material, photoelectric absorption dominates in energies below  $\sim 0.8$  MeV, Compton scattering in energies between  $\sim 0.8$  MeV and  $\sim 7$  MeV, and pair production in energies above  $\sim 7$  MeV.

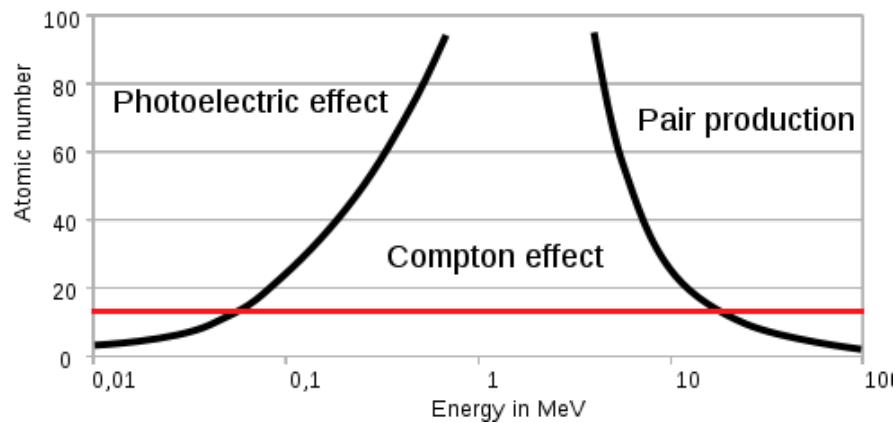


Figure A.4: Main attenuation effects of x-rays depending on energy and atomic number<sup>4</sup>.

For  $^{60}\text{Co}$  the two gamma energies are 1.17 and 1.33 MeV [4] and the interacting material is silicon which has an atomic number of 14, shown with a red line in Figure A.4. Therefore the dominating interaction with matter is in the Compton scattering region.

## A.2 Leksell Gamma Knife<sup>®</sup>

The Leksell Gamma Knife<sup>®</sup> (LGK) uses the radioactive decay of  $^{60}\text{Co}$  to perform non-invasive radiosurgery on the patient. The working principle behind LGK radiosurgery is that about 200 beams of gamma radiation intersect in a focus point creating an isocentre that has an intensity 200 times the intensity

<sup>4</sup><https://commons.wikimedia.org/wiki/File:XraY-shielding.svg>

of a single beam. At the location of the focus point (Figure A.5) the total energy deposition is significantly higher than in the surrounding tissue, therefore the targeted tissue can be irradiated without substantially damaging adjacent normal brain tissue.

### A.2.1 Placement of sources and collimators

A collimator is a device which narrows a radiation beam to a specific width as well as focusing the radiation beams so they are parallel. The collimators in the LGK have 3 different sizes: 4mm, 8 mm and 16 mm, where the dimensions are approximately the geometrical dimensions of the final beam in air. The availability of different collimator sizes allows for flexibility when planning the dose delivery to different target size and target geometry.

The number of  $^{60}\text{Co}$  sources, and therefore the number of collimators, depends on the LGK model; 192 for Perfexion<sup>TM</sup> and 201 for LGK B and LGK C. Though LGK B and LGK C are obsolete LGKs and are currently not supported by Elekta Instrument AB (Elekta). The sources and collimators for the LGK Perfexion are distributed  $360^\circ$  around the target in 8 different sectors, as shown in Figure A.5. Each sector can be moved so that the sources align with the chosen fixed collimator size [6], see Figure A.6 or so that the sources are closed off completely.

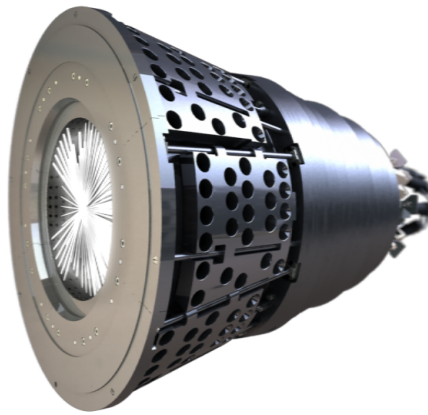


Figure A.5: Collimator body with one sector moved and showing intersecting gamma rays to a focus point. Courtesy of Elekta Instrument AB.

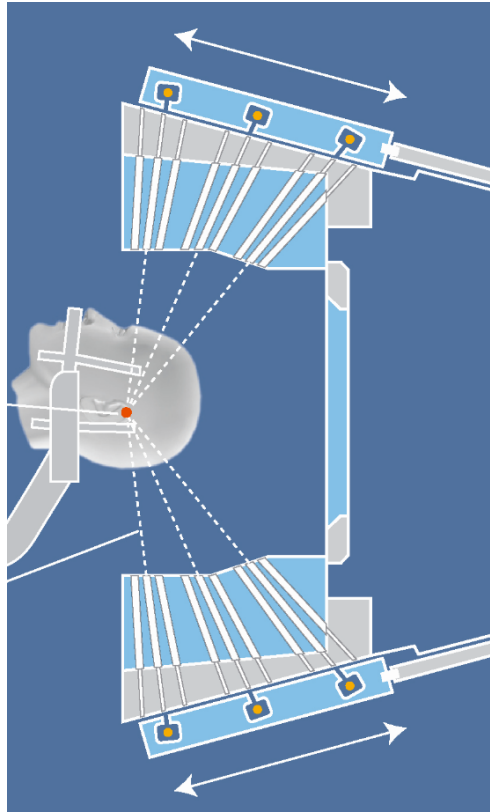


Figure A.6: Image showing intersecting gamma rays (dotted lines) in a red focus point in a patient. Arrows show available movement of collimator. Orange represents  $^{60}\text{Co}$  sources. Courtesy of Elekta Instrument AB.

The sources are located in these sectors in five separate rings with different Z-positions. Since all beams intersect in the focus point, see Figure A.6, each ring has its unique angle with the vertical plane. The vertical plane can be observed in Figure A.7. For example, for the 8 mm collimator the angles are  $11.57^\circ$ ,  $21.31^\circ$ ,  $27.77^\circ$ ,  $36.78^\circ$  and  $42.47^\circ$ . The number of sources in each ring are different due to the shape of the collimator body, and the fact that all beams intersect in the focus point.

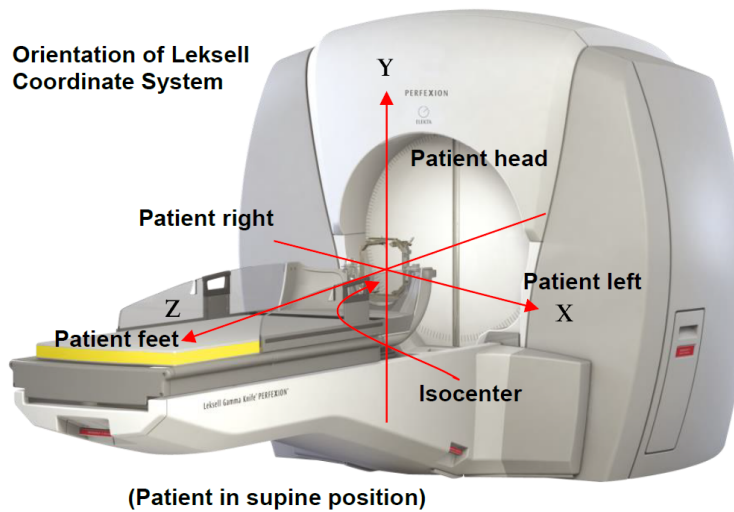


Figure A.7: Orientation of Leksell system coordinates for Leksell Gamma Knife<sup>®</sup>. Patient in supine position. Courtesy of Elekta Instrument AB.

### A.2.2 Movement of the patient

The movement of the patient is controlled by the Patient Positioning System (PPS). The PPS is the couch the patient lies on and controlled to certain positions in the LGK. This in order to change the position of the isocenter to the tumours position. The PPS is required to have a very high mechanical stability as well as accuracy during movement [14].

The PPS will be used in the experiments in order to move the detector forward into the LGK and therefore in a decreasing Z-direction, see Figure A.7.

## A.3 Noise

Noise is considered a spontaneous fluctuation in either current or voltage and can happen in multiple places of a circuit. For example in a semiconductor. In a semiconductor this noise is always present and could be multiple entities, such as thermal noise or shot noise. Thermal noise occurs due to random motion of charge carriers due to thermal excitation. This leads to a difference in current/voltage. Shot noise is caused by a potential barrier which can be overcome by the carriers with higher energy, causing noise. This means that when having a semiconductor detector in a dark room with no radiation applied to the detector, a signal will still be formed [23].

## A.4 Setup for radiation detection

The setup of measuring and visualizing the amount of  $^{60}\text{Co}$  sources in a Leksell Gamma Knife<sup>®</sup> contains multiple parts.

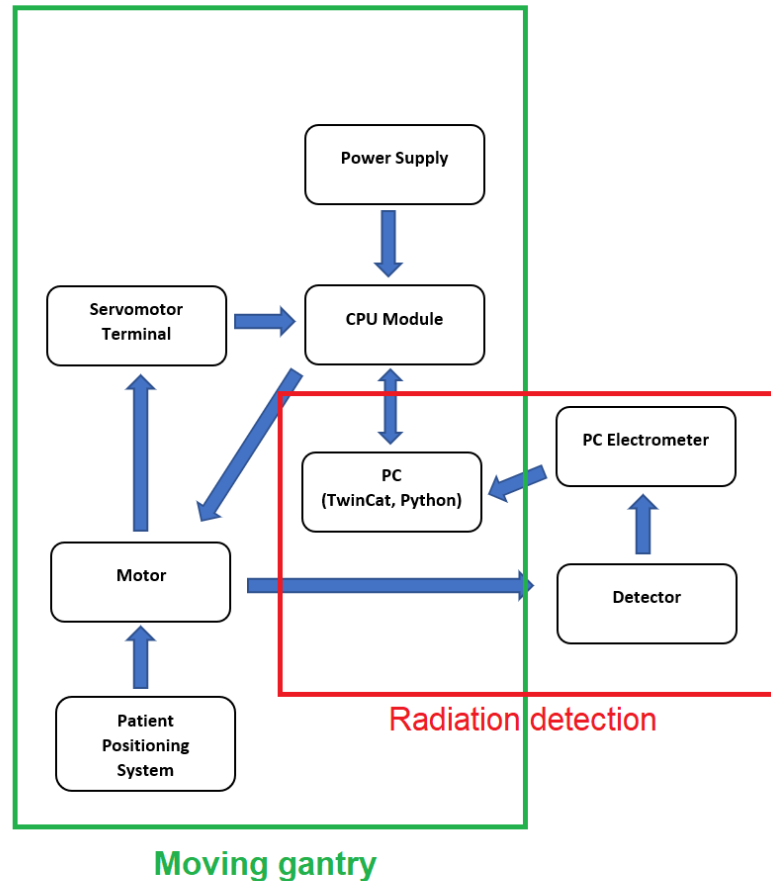


Figure A.8: Block diagram showing all parts of the radiation detection block and the moving gantry block as well as their respective connection.

A motor setup is connected to a servomotor terminal, which sends information through a CPU module powered by a power supply. Attached to the motor is a rod which contains a detector circuit attached to it containing a detector connected to an electrometer which then is connected to a PC. The purpose of the setup is to move the photodiode in a circular motion in order to gather radiation data from all available source positions in the Leksell Gamma Knife<sup>®</sup>.

To move the detector in a Z-direction (Figure A.7) the LGKs integrated patient positioning system is used, as explained in Section A.2.2. All of this is explained in the block diagram shown in Figure A.8.

### **A.4.1 Motor**

The motor, which should be used for controlling the detection setup toward every source location, needs to have certain characteristics. It must have a compact design so that the full setup does not become too big. The motor also needs to have a simple connection to a computer in order to be able to control it, preferably from a distance so that the computer can be controlled a far distance from the Leksell Gamma Knife<sup>®</sup>. Apart from these specifications the motor needs to have a software able to control precise movements in order to move the detector to specific coordinates where the sources are located.

### **A.4.2 Detector types**

The gamma radiation detection could be done in multiple ways with multiple kinds of detectors. Listed below are a few examples of devices which could detect radiation.

#### **A.4.2.1 Scintillator with a photomultiplier tube**

A scintillator with a connecting photomultiplier tube (PMT) could be used for detecting gamma radiation [1]. When a scintillator is hit by a particle, the scintillator absorbs its energy and releases visible particles in the form of light. This visible light then enters the PMT which serves as an amplifier. The photons energy will be transferred to multiple electrons, each multiplying along the path of the tube. This provides a current at the end of the path which is able to be measured [7].

#### **A.4.2.2 Solid-state detector**

A solid-state detector is a high performing detector device [21] with the ability to detect gamma radiation [16]. The solid-state detector detection is done by the use of for example a semiconductor.

A semiconductor material is defined by its electrical properties, where the electrical conductivity lies between that of metals and insulators. Electrical

conductivity determines a materials ability to conduct an electric current. Examples of commonly used semiconductor materials for radiation detectors are silicon and germanium. The chosen material also has the possibility to be doped. Doping means introducing impurities into the material in order to provide improved electrical properties such as the materials conductivity [11]. This is how for example diodes are created.

Semiconductors are exceptional in the application of detecting radiation. The reason for this is that the density of semiconductors is high. This means that substantially more atoms exist to interact with and thereby providing more measurable current in a smaller design. Therefore the dimensions can be kept small compared to for example gaseous detectors [11]. The efficiency of semiconductor detectors may have angular dependencies which are inversely proportional to the energy of the incoming radiation [17].

The bandgap is a key property of a semiconductor, which is the energy difference between the valence band and the conduction band. The value for the bandgap for semiconductors usually lies between 0.4 and 4 eV [10]. When radiation such as gamma rays interacts with a semiconductor, see A.1.2.1, A.1.2.2 and A.1.2.3, part of its energy, typically a few eV, is absorbed by the electron which then migrates from the valence band to the conduction band. This generates a corresponding hole where the electron existed in the valence band. This is called ionization [10]. These holes are then filled by electrons which generate a flow of current [11].

The electron in the conduction band is then made to drift under the influence of an applied electric field. The hole, representing a net positive charge, will also tend to move in an electric field, but in a direction opposite that of the electron. The motion of both of these charges contributes to the observed conductivity of the material.

### **A.4.3 Electrometer**

An electrometer is a calibrated and accurate system which measures low current obtained from a connected detector. This current is later on amplified.

A specific electrometer used for radiation calculation is the PC Electrome-

ter, developed by Sun Nuclear corporation and shown in Figure A.9. This is a portable electrometer which receives, amplifies the current and sends the information through a connected USB cable to a PC. The electrometer has a specified acquisition time initially set to 500 ms [18] which can be altered to a minimum of 25 ms. Included with the PC Electrometer is a radiation calculating software created by the same company, explained further in Section A.4.3.1.

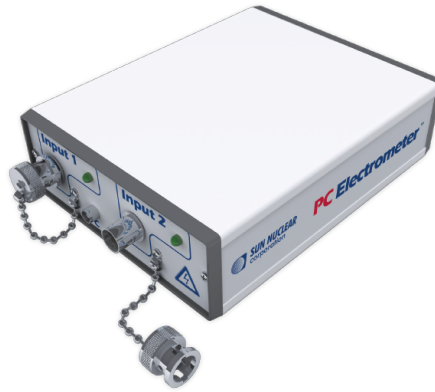


Figure A.9: PC Electrometer from Sun Nuclear corporation [18].

#### A.4.3.1 PC Electrometer Software

The PC Electrometer software (PCE 1DS), see Figure A.10, presents the measured energy deposition during the integration time in coulombs. In order to reduce the amount of background radiation noise, a background correction factor is calculated in the software by gathering the mean current value from a chosen time period of 15/30/45/60 seconds and subtracting it from the measured current. The necessary information from the software, such as radiation in coulomb and elapsed time, can be exported to a separate specified text file which will be continuously updated with the new corresponding values. The text file is updated every 4 seconds with all the values in those 4 seconds, separated by a time corresponding to the specified acquisition time.

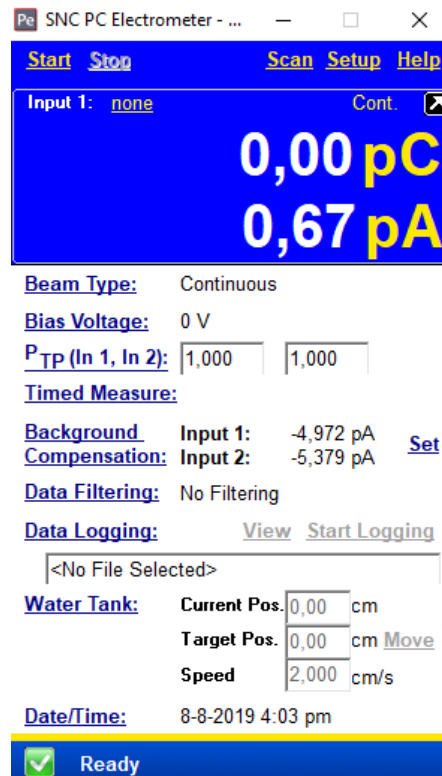


Figure A.10: Screenshot of PCE 1DS software from Sun Nuclear corporation.

#### A.4.4 EtherCAT

EtherCAT, developed by Beckhoff, stands for Ethernet for Control Automation Technology and is an industrial Ethernet technology with very high flexibility regarding its possibilities. Ethernet is a system for connecting computers in order to create a local area network and therefore pass information easily. The EtherCAT technology is an open technology, which means that anyone can use it or implement it. It works by having all necessary items connected to the EtherCAT system and when reading the data, EtherCAT reads node by node and writes data back simultaneously. This makes the EtherCAT technology have really high performance since it does not have to wait for information to return before it can send. The fast reaction times of the EtherCAT technology enables a reduction in the waiting times before any occurrence. The technology is very simple and robust and works well in controlling for example a motor to a specific position with high accuracy and at a fast pace [5].

The list of what can be used with the EtherCAT technology is very long and

everything has an easy connection with how the parts are formed and connected to each other. This enables easy changes to the structure of the device connected with EtherCAT [5].

The system works well for high precision movement for motorised systems [19]. Adding to this the communication setup is also from the same company as the motor setup which enables easy integration and problem solving if any issues arise.

#### **A.4.5 TwinCAT**

TwinCAT, developed by Beckhoff and stands for "The Windows Control and Automation Technology", is a software system which transforms a computer into a real-time controller with a system of multiple Programmable Logic Controllers (PLC) and a corresponding programming environment. The software connects all the devices and enables control of for example motors or other automatic technology. The controlling of the PLCs is done with multiple programming languages from the 3<sup>rd</sup> edition of the IEC 61131-3 standard, such as Instruction List, Ladder Diagram, Function Block Diagram, Sequential Function Chart and Structured Text [9]. TwinCAT eXtended Automation Engineering is the software in which the control is performed and this program is integrated with Microsoft Visual Studio®. This makes it possible to program automation objects in parallel with the aid of other programming languages such as C, C++ or the IEC 61131-3 standard [22].

Through TwinCAT a development of the movement pattern of the motors can be made, controlling the motors motion and absolute position. By controlling the system with a computer the data collection can be done simultaneously as well as getting feedback on and controlling the motion of the PPS.

#### **A.4.6 <sup>60</sup>Co setup for experiments**

Performing tests and experiments on the detection setup is essential in knowing if it has the capability of working in a complete setting. Elekta has multiple available gamma knives but neither of these are loaded with any <sup>60</sup>Co sources. Only one radioactive <sup>60</sup>Co source available for laboratory setups exist for Elekta to use. This is where some of the experiments will be conducted, whereas the rest of the testing will be conducted at Karolinska Universitetssjukhuset in Solna.

In this room a radioactive  $^{60}\text{Co}$  source exist, located inside a steel shell filled ball of lead. This is to reduce the exposure of radiation to the surroundings in the room [13]. The ball has an opening inside of it which is connected to the outside of the ball. This is where the  $^{60}\text{Co}$  source is located. Apart from this, the source is shifted a distance perpendicular to the direction of the hole to reduce the external radiation. Inserted in the opening while not operating is a lead plug.

When one experiments with the radiation from the source, one removes the lead plug, which increases the radiation slightly. After this one could turn a knob which moves the source perpendicularly to the opening and therefore increases the radiation to its full effect. One could also place a collimator inside this ball in order to only have a certain opening diameter.

#### **A.4.7 Dose limit**

The dose limit recommendations for body exposure to radiation is recommended by the Swedish parliament. Where the limit for employees over 18 years old and working with ionizing radiation, should not exceed 20 mSv effective dose in any single year [20]. This value follows the recommendations from the International Commission on Radiological Protection [8].

### **A.5 Radiation beam profile**

The shape of a beam profile is as depicted in Figure A.11. The penumbra is the region of steep dose rate decrease at the edge of a radiation beam, it is normally defined as the distance between the points 80% of max dose and 20% of max dose at a specific distance from the source [2]. An increase in the penumbra provides a wider non-rectangular beam profile [3]. One factor that also provides this beam profile is the setup. Due to the source being blocked by a collimator, some radiation will pass through the collimator or scatter and therefore hit the detector, but with a decreased energy due to Compton scattering, explained in Section A.1.2.2.

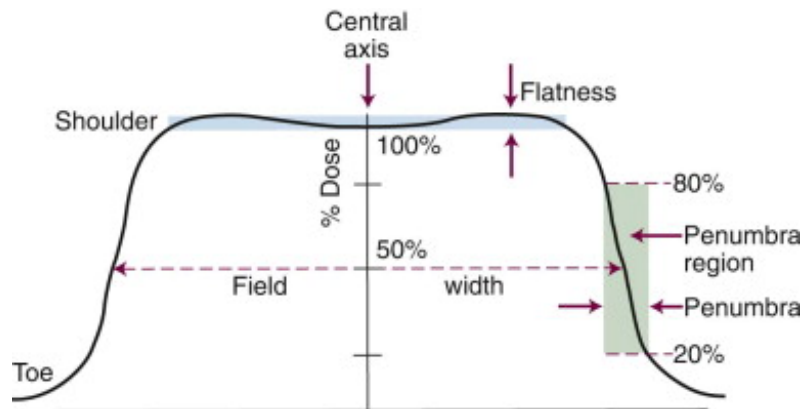


Figure A.11: The dose profiles of a typical photon beam are characterized by shoulder and toe regions, with definitions for field width, flatness, and penumbra as indicated<sup>5</sup>.

One of these factors, is the partial volume effect on the detector. When moving the detector across a radiation field, firstly only a part of the detector is hit by the radiation and not the whole detector. Because of this, a smaller amount of radiation hits the detector. When moving further through the field the radiation increases to a peak and when moved through the center of the peak the radiation decreases.

### A.5.1 Inverse square law

The inverse square law is the decrease in the intensity of the radiation from a source with the square of the distance, explained by Equation A.3 [2].

$$intensity \propto \frac{1}{d^2} \quad (A.3)$$

This indicates that if a detector is, for instance, 3 times further away from a source, the intensity decreases ninefold.

<sup>5</sup>Reprinted from Clinical Radiation Oncology , third edition, J. Daniel Bourland, Radiation Oncology Physics, 95-152, 2012, with permission from Elsevier.

# Bibliography

- [1] Becker, E. M et al. “Small Prototype Gamma Spectrometer Using CsI(Tl) Scintillator Coupled to a Solid-State Photomultiplier”. eng. In: *IEEE Transactions on Nuclear Science* 60.2 (2013), pp. 968–972. ISSN: 0018-9499.
- [2] Beyzadeoglu, Murat, Ozyigit, Gokhan, and Ebruli, Cuneyt. *Basic Radiation Oncology*. eng. Berlin, Heidelberg: Springer Berlin Heidelberg, 2010. ISBN: 9783642116650.
- [3] Bourland, J. Daniel. “Chapter 6 - Radiation Oncology Physics”. In: *Clinical Radiation Oncology (Third Edition)*. Ed. by Leonard L. Gunderson and Joel E. Tepper. Third Edition. Philadelphia: W.B. Saunders, 2012, pp. 95–152. ISBN: 978-1-4377-1637-5. DOI: <https://doi.org/10.1016/B978-1-4377-1637-5.00006-7>. URL: <http://www.sciencedirect.com/science/article/pii/B9781437716375000067>.
- [4] Drzymala, R. E. et al. “Angular measurement of the Cobalt-60 emitted radiation spectrum from a radiosurgery irradiator”. In: *Medical Physics* 28.4 (2001), pp. 620–628. DOI: 10.1118/1.1355305.
- [5] *EtherCAT - The Ethernet Fieldbus*. Brochure. 2018. URL: [https://www.ethercat.org/download/documents/ETG\\_Brochure\\_EN.pdf](https://www.ethercat.org/download/documents/ETG_Brochure_EN.pdf).
- [6] Ganz, Jeremy C. *Gamma Knife Neurosurgery*. Springer Vienna, 2011. DOI: 10.1007/978-3-7091-0343-2.
- [7] Gupta, Tapan K. *Radiation, Ionization, and Detection in Nuclear Medicine*. eng. 2013. ISBN: 3-642-34076-8.
- [8] ICRP. “Preface, Executive Summary and Glossary”. In: *Annals of the ICRP* 37.2-4 (2007), pp. 9–34. DOI: 10.1016/j.icrp.2007.10.003.

- [9] John, Karl Heinz. *IEC 61131-3: Programming Industrial Automation Systems Concepts and Programming Languages, Requirements for Programming Systems, Decision-Making Aids*. eng. 2nd ed.. 2010. ISBN: 3-642-43694-3.
- [10] Johnston, Allan. "Semiconductor Fundamentals". eng. In: *Reliability And Radiation Effects In Compound Semiconductors*. World Scientific Publishing Co. Pte. Ltd., 2010, pp. 9–40. ISBN: 9789814277112.
- [11] Knoll, Glenn F. *Radiation detection and measurement; 4th ed.* New York, NY: Wiley, 2010.
- [12] Kunz, Robert G. "Radioactive Decay". eng. In: *Environmental Calculations*. Hoboken, NJ, USA: John Wiley & Sons, Inc., 2010, pp. 468–506. ISBN: 9780470139851.
- [13] Nelson, G and Reilly, D. "Gamma-Ray Interactions with Matter". In: *Passive Nondestructive Analysis of Nuclear Materials*. Los Alamos National Laboratory, 1991. Chap. Gamma-Ray Interactions with Matter, pp. 27–42.
- [14] Novotny Jr., J. et al. "Long-term stability of the Leksell Gamma Knife® Perfexion™ patient positioning system (PPS)". In: *Medical Physics* 41.3 (2014), p. 031711. doi: 10.1118/1.4866225.
- [15] Radiation Products Design, Inc. *Cables, chambers accessories*. URL: [https://www.rpdinc.com/Q-Cables\\_Chambers\\_Accessories.pdf#page=17](https://www.rpdinc.com/Q-Cables_Chambers_Accessories.pdf#page=17).
- [16] Ryzhikov, V. D et al. "Detection of gamma-neutron radiation by novel solid-state scintillation detectors". eng. In: *2015 4th International Conference on Advancements in Nuclear Instrumentation Measurement Methods and their Applications (ANIMMA)*. IEEE, 2015, pp. 1–5.
- [17] Stansook, Nauljun et al. "Technical Note: Angular dependence of a 2D monolithic silicon diode array for small field dosimetry". In: *Medical Physics* 44.8 (2017), pp. 4313–4321. ISSN: 0094-2405.
- [18] Sun, Nuclear corporation. *PC Electrometer*. URL: [https://www.sunnuclear.com/documents/datasheets/pc\\_electrometer.pdf](https://www.sunnuclear.com/documents/datasheets/pc_electrometer.pdf).
- [19] Sung, M. et al. "An EtherCAT-based motor drive for high precision motion systems". In: *2011 9th IEEE International Conference on Industrial Informatics*. July 2011, pp. 163–168. DOI: 10.1109/INDIN.2011.6034856.

- [20] Swedish Code of Statutes, Sveriges Författningsförsamling. “Strålskyddsförordning (2018:506)”. In: (2018).
- [21] Tsuchiya, Katsutoshi et al. “Basic performance and stability of a CdTe solid-state detector panel”. In: *Annals of Nuclear Medicine* 24.4 (May 2010), pp. 301–311. ISSN: 1864-6433. DOI: 10.1007/s12149-010-0354-1.
- [22] *TwinCAT 3 | eXtended Automation (XA)*. Brochure. 2012. URL: [https://download.beckhoff.com/download/document/catalog/Beckhoff\\_TwinCAT3\\_042012\\_e.pdf](https://download.beckhoff.com/download/document/catalog/Beckhoff_TwinCAT3_042012_e.pdf).
- [23] Wilamowski Bogdan. David Irwin, J. “Noise in Semiconductor Devices”. eng. In: *The industrial electronics handbook*. The electrical engineering handbook series. Boca Raton, Fla.: CRC, 1997. Chap. 11. ISBN: 0-8493-8343-9.





TRITA CBH-GRU-2020:111